DOI: 10.13009/EUCASS2023-044
Aerospace Europe Conference 2023 – 10TH EUCASS – 9TH CEAS

Investigation of seated passenger's vibration using a full-flight simulator

Antonio Esposito[⋆†], *Calogero Orlando*[⋆] *and Andrea Alaimo* [⋆]
[⋆]*Kore University of Enna, Faculty of Engineering and Architecture*
Mediterranean Aeronautics Research & Training Academy, 94100 Enna (EN), Italy
antonio.esposito@unikore.it · calogero.orlando@unikore.it · andrea.alaimo@unikore.it
[†]Corresponding author

Abstract
Vibrational problems in aircraft are of great importance for the comfort and well-being of occupants. In this work, a preliminary experimental campaign is carried out using a full flight simulator to obtain measurements of the acceleration transmitted from the seat to the passengers during some selected flight segments. It considers the take-off including the initial climb, the final approach including the touchdown, and two cruise segments with and without turbulence effects. Specifically for the cruise phase, the power spectral density calculated from the seat surface accelerations was compared with literature and real flight data to verify the simulator's capability. The comfort indexes are calculated according to the current ISO 2631 standard for characterizing the effects of vibrations. Two types of seat configurations are studied. The results conclude that the evaluation of comfort indexes in an advanced simulated environment, not merely based on objective data, can contribute to the research of new comfortable scenarios inside the cabin.

1. Introduction

In 2002, the EU Council introduced an act that regulates the minimum requirements for protecting workers from exposure to mechanical vibration sources.[1] Studies and research are being carried out to identify the problems associated with human exposure to vibrations transmitted by motor vehicles or other sources of vibration. The studies so far focused not only on the medical assessments related to body damage due to exposure[2,3] but also on mechanical and mathematical modeling attempts[4–7] to indirectly evaluate the stresses transmitted to the seat and, therefore, to the humans.

In this framework, the term whole body vibration (WBV) is used when the entire body is subjected to vibration and its effects. Contrary to what happens in the evaluation of local vibration, in which one or more parts of the human body (such as the head or arms) are exposed to vibration, the WBV affects the whole body and is therefore considered because its effects can be transmitted within the individual. Several aspects have a significant impact on the body's response to the inputs it receives, but the most important is undoubtedly the interface with the seat;[8–10] in fact, many environments can cause the WBV, among these, all transportation vehicles must be considered. It is common for people to experience WBV on most days of their lives, i.e. persons may travel in a car, a bus, a train or may fly in aircraft or travel in ships.[11–15] Astronauts, jockeys, race car drivers, and cabin crew may be exposed to WBV; in these and many other environments, people are primarily exposed to vibration while seated and are exposed to a wide range of vibration magnitudes, waveforms, and duration. WBV occurs when people stand on vibrating surfaces and the vibrations affect parts of the body also away from the point of exposure. For example, when driving over a bumpy surface, the vibration is transmitted through the vehicle to the seat.[16] In turn, the vibration is transmitted through the body of the driver to the head.

With regard to aviation, it should be noted that pilots and flight crews are constantly exposed to vibrations in their operating environments.[17,18] In this regard, vibrations can profoundly affect pilots inside the cockpit, altering their psychophysical state, especially in the case of long-haul flights. For both fixed-wing and rotary-wing platforms, prolonged sitting posture, daily flight hours, or cumulative vibration and WBV dose can strongly correlate with psychophysical discomfort.[7,12] In addition to the personal health implications, the combination of these conditions can also cause decreased alertness and situational awareness, thus impacting overall mission performance.[19] During a flight, vibrations can also affect the passengers, and the phenomenon can mainly be related to a component felt as a discomforting effect.

DOI: 10.13009/EUCASS2023-044

People are constantly traveling for many reasons, and among the transportation systems, air travel represents an increasing opportunity for airlines. Passengers' choice lies first on direct flights, time, and price, then on aspects such as marketing and comfort, past experiences, and delays. Increasing comfort can therefore attract more passengers and can determine an increasing revenue for airlines.[20]
Comfort is in most cases related to a subjective sense of well-being and can be defined as a state of physiological, psychological, and physical harmony between human beings and the environment that surrounds them. This subjectivity complicates the engineering of comfort because it is not possible to predict individual reactions to a particular stimulus. Despite this difficulty, it is possible to design the comfort of a passenger cabin by performing some important preliminary steps in the initial phase of the project such as, for example, the evaluation of passenger comfort based on different cabin layouts in terms of lining, ergonomics, microclimate, levels of noise and vibration and ambient lighting.[21] In fact, despite the technological innovations that can be made to the passenger cabin of an airplane, the crucial point is always the subjective assessment from passengers. For this reason, several studies have been conducted to investigate the influence of some key elements on the sensation of comfort perceived by passengers during the flight.[22]
With regard to the transmission of seat vibrations, uniaxial sinusoidal signals have been used in laboratory studies in the past due to the methodological difficulties of using complex multi-axial stimuli.[23,24] However, the use of motion system simulations now makes it possible to characterise the phenomenon in all its complexity.[9,25,26]
While it is particularly difficult to validate subjective data for each level of vibration transmitted to the body, it is worth noting that many passengers experience seasickness, car sickness, or air sickness. These can be broadly categorized as different forms of motion sickness and could be used as comfort indicators. All environments characterized by such sickness share the common element of real or apparent motion. The term 'sickness' implies a medical problem, but motion sickness is a normal and natural reaction to some forms of movement. Its ultimate effects may lead to the need for treatment, but motion sickness itself is not directly dangerous. A problem often associated with motion sickness is a state of apathy, impaired performance, or both, which could lead to an increased likelihood of errors of judgement. Therefore, it is appropriate to analyze the two elements of motion sickness: the physiological response to motion, associated with wave motion and visual instability, and the psychological response, whose symptoms can be alleviated by entertainment.[27]
On this basis, an experimental campaign is performed in order to evaluate the objective comfort indexes of two different seat configurations under different dynamic input corresponding to different flying segments. To do this, a Full Flight Simulator (FFS) that replicates the behavior of a business jet aircraft with the highest level of accuracy is used.
In what follows, section 2 describes the experimental set-up, with details on the motion system and tools used for data acquisition, while in section 3, the indexes considered and related results are reported and commented on.

2. Materials and Methods

2.1 Full Flight Simulator

In an FFS, one of the main components is the motion system, commonly characterized by its maximum excursions, speeds, and accelerations for each degree of freedom. It is essentially a six degrees of freedom platform (Stewart Platform or Hexapod) which, through the coordinated and simultaneous motion of six hydraulic or electric actuators, allows the reproduction of linear displacements (heave, sway and surge) and rotations (pitch, roll and yaw). The FFS, installed at the MARTA Centre (Mediterranean Aeronautics Research & Training Academy), mounts an eM6-1400-14000 full electric six degrees of a freedom motion system with a gross moving load of up to 14000 kg, designed for use in FAA, EASA Level D and ICAO 9625 type VII flight simulation systems for both fixed wing and rotary wing aircraft. It consists of six identical electric actuators, which comprise a ball screw driven by a brushless DC servo motor. Technical specifications in terms of excursions, velocity and acceleration is detailed in Table 1.
A dedicated motion base interface software receives various data from the simulation. The motion base interface software interprets the simulation data and generates commanded cues and special effects that are sent to the motion base. The communication among simulation computers and motion real-time computer is carried out with the simple datagram-based UDP-messages. Regular communication includes the system's operational state and vehicle dynamic data, needed by the cueing algorithm. The host update rate is always kept above 60 Hz for smooth cueing. Examples of cues and special effects generated are not limited to linear accelerations, velocities, and rotational accelerations; additional realistic effects are simulated as the engine vibrations in flight, stall buffet, gear door extension/retraction, landing bump, and many more.
As the motion cues are limited to the maximum displacement and velocity of the actuators, subjective tuning sessions were performed together with type-experienced pilots to match the cues as close as possible to the experience in the real aircraft.

DOI: 10.13009/EUCASS2023-044

Table 1: Technical specifications of the eM6-1400-14000 motion system.

	Excursions			Velocity		Acceleration	
	single DOF	non-single DOF					
Surge	-1.17/1.40	-1.50/1.50	m	0.97	m/s	7.1	m/s^2
Sway	-1.17/1.17	-1.50/1.50	m	0.97	m/s	6.5	m/s^2
Heave	-0.87/0.87	-0.87/0.87	m	0.97	m/s	7.8	m/s^2
Roll	-27/27	-30/30	deg	20	deg/s	140	deg/s^2
Pitch	-29/33	-32/35	deg	22	deg/s	150	deg/s^2
Yaw	-29/29	-37/37	deg	23	deg/s	240	deg/s^2

2.1.1 Simulated Motion compared to Real Flight

Considering that the use or disclosure of source data used for the Main Qualification Test Guide (MQTG) of FFS is subject to restriction and may not be reproduced, and since just one flight data records of accelerations are freely available for the simulated aircraft, a comparison with literature available by Catherines et al.[28] is proposed in the current work. The authors are fully aware that for experimental purposes, a single data collection cannot be considered statistically significant; therefore, Catherines et al.[28] data are assumed as reference values to compare power spectral density (PSD) shown in Figure 1 and root mean square (RMS) and max peak (Δn) acceleration values listed in Table 2. Technical report by Catherines et al.[28] presents PSD, RMS, and Δn data collected during different flight phases on civil aircraft. Several runs with two different conventional take-off and landing (CTOL) aircraft, CTOL-1 a three-engine aircraft, and CTOL-2 a double-engine, are presented. Regarding the cruise phase, data were recorded at constant altitudes during rough cruises (CR) and smooth cruises (CS). The data represent measurements obtained at the c.g. position and also at the forward position of the aircraft.

Concerning the real flight, the authors recorded the data on CESSNA Citation 560 XLS aircraft during a private flight. Specifically, data were gathered during a cruise segment in level flight at an altitude of 32000 ft for flight LWG291-LICC-LIRA performed on 24/04/2019. The data were recorded using a WT901SDCL acceleration data logger employed in a stand-alone configuration. The sensor can collect data on an external Micro Secure Digital card. The acquisition sampling rate was set to 200 Hz. The sensor was positioned on the seat of a 72 kg, 1.75 m, 36 year old male passenger in the forward seat position of the aircraft cabin.

PSD illustrated in Figure 1 along with RMS and Δn values listed in Table 2 for the Citation 560 XLS are comparable with the rough cruise presented by Catherines et al.[28] The RMS value of the Citation 560 XLS is higher than CR CTOL-1, contrary to the Δn, which presents a lower value. Overall, the data collected during the flight in the Cessna Citation can be considered analogous to a rough cruise, as given by Catherines et al.

In order to evaluate the performance of the simulator in replicating the real flight behaviour and to reproduce a similar seat configuration, data were recorded at seat B of the FFS simulator (refers to Figure 3). The results in terms of PSD during flight with and without turbulence are shown in Figure 2. They are compared with the rough cruise recorded on the Citation XLS 560. It is worth noting that data are only for vertical acceleration. The results show a good agreement between the experimental data and the simulated behavior in the range considered from 1 to 10 Hz.

Table 2: Comparison of root mean square (RMS) and Max Peak acceleration (Δ n) values for Cessna Citation 560 XLS cruise segment with Catherines et al.[28] literature data.

	Catherines et al. [24] Mean (Standard Deviation)				
	CR CTOL-1	CR CTOL-2	CS CTOL-1	CS CTOL-2	CR Citation 560 XLS
RMS	0.042 (0.006)	0.042 (0.012)	0.006 (0.001)	0.006 (0.001)	0.063
Δ n [g]	0.225 (0.046)	0.220 (0.051)	0.019 (0.004)	0.023 (0.003)	0.166

DOI: 10.13009/EUCASS2023-044

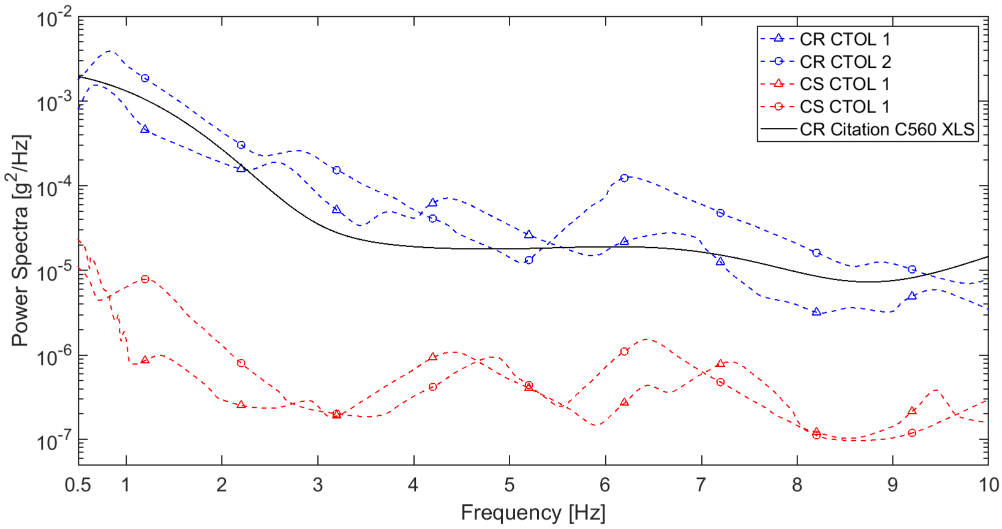

Figure 1: Power Spectral Density of accelerations measured during the Citaton flight on cabin seat with a passenger (black line) compared with Catherines et al.[28] literature data.

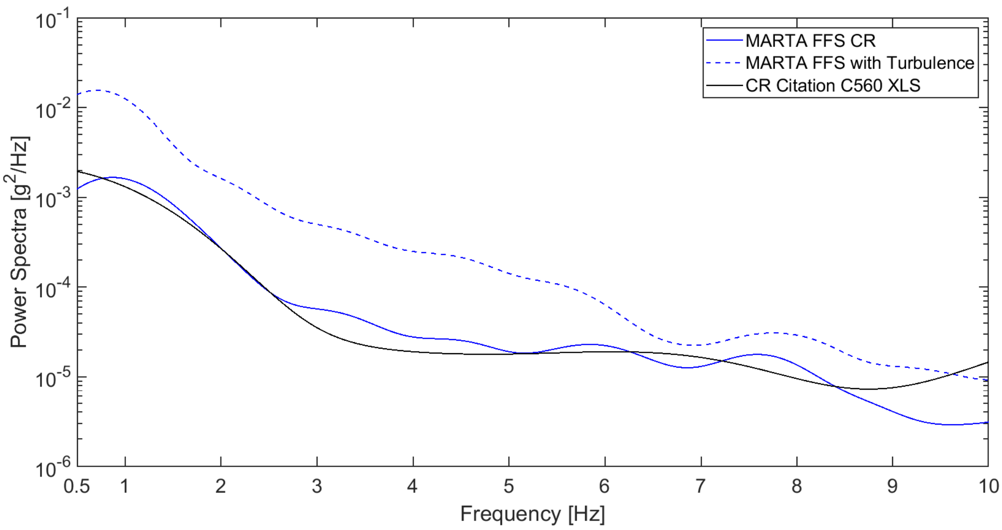

Figure 2: Power Spectral Density of accelerations measured during simulated cruise phase on MARTA FFS with moderate turbulence (blue dashed line) and without turbulence (blue line) compared with real flight data (black line).

2.2 Simulated Flight Phases

The WBV analyses presented in the successive results, investigate three different flight conditions: take-off, landing, and cruise. In particular, missions for the cruise phase are performed with and without turbulence according to the previous comments. No details by the FFS manufacturer about the turbulence model implemented in the simulator software are available. Nevertheless, based on the values of the root mean square value for vertical acceleration and max peak value, according to Huobolt,[29] it is possible to classify the turbulence severity as moderate. In Table 3 mean and standard deviation values measured on vertical accelerations during the simulated flights are listed and compared with the range for the category of moderate turbulence. It is worth noting that the values recorded on MARTA FFS flight simulations are within the range defined by Huobolt both for root mean square and max peak.

Regarding the flight segments, the take-off phase lasts 3 min; the phase starts 10 s before the brake release. After about 35 s, the lift-off phase occurs, and from this point, the other 2 min of data are recorded during the climb. The cruise phase data are acquired in level flight for 3 min, first without turbulence and during the second phase with moderate turbulence. The last flight phase analyzed is the landing; in this phase, the acquiring time equals 3 min. The segment starts 10 s before the approach from 5 nautical miles with the aircraft positioned into the ILS flight path. After about

DOI: 10.13009/EUCASS2023-044

Table 3: Classification of simulated turbulence severity, root mean square (σ) and peak (Δn) values for vertical acceleration.

	Simulator cabin floor	**Houbolt[29]**
	Mean (Standard Deviation)	Classification for moderate range
RMS	0.246 (0.021)	0.2 ÷ 0.35
Δ n [g]	0.967(0.083)	0.6 ÷ 1.05

150 s, the touchdown occurred; data were acquired during the landing run until the parking brake was set. Additional data on flight phases and maneuvers performed are available in.[30,31]

2.2.1 Seat Configuration and Accelerometers Arrangement

Two different seat configurations are taken into account. As shown in Figure 3 (a), the seats located in the Non-Simulated Area (NSA) of the simulator are different (the NSA is part of the simulator that does not narrowly replicate the real aircraft) in particular, the seat named with the acronym "A" is very similar to an attendance crew seat. Instead, the seat marked with "B" is representative of a business configuration.

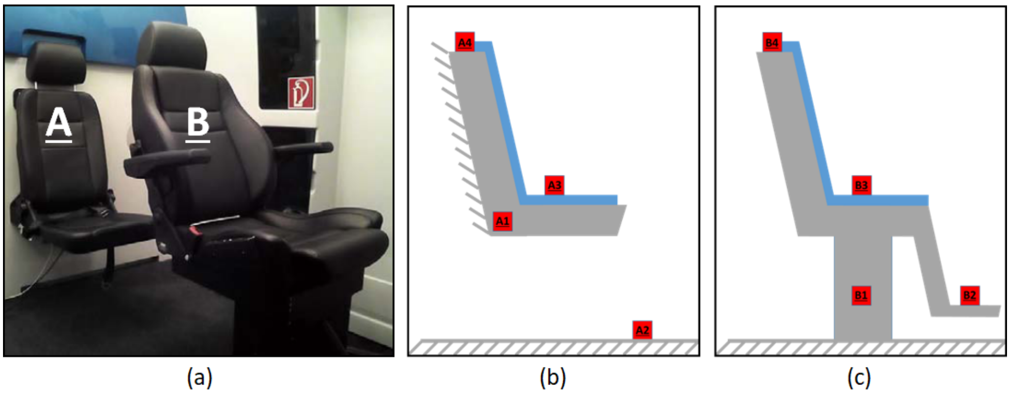

Figure 3: Seat layout and named identification (a), Accelerometers arrangement for Seat A (b) and Seat B (c).

The seats installed in the NSA are K310 series manufactured by König Komfort-und Rennsitze GMBH. The seats are not strictly for aeronautical purposes; however, they are used for high comfort levels in luxury cars. For the sake of completeness, a scheme of the main dimensions characterizing the seats is presented in Figure 4 and reported in Table 4.

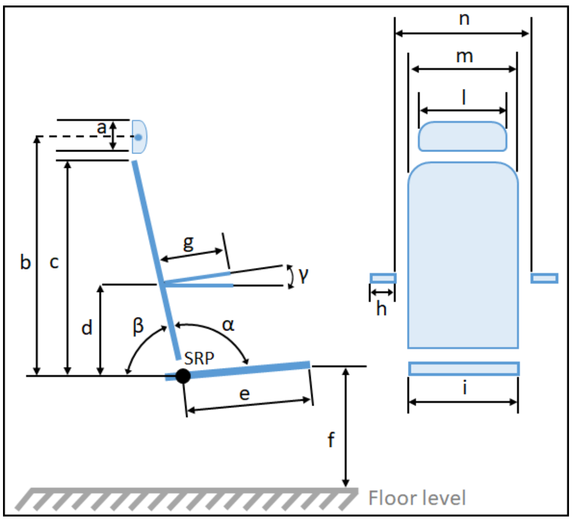

Figure 4: Measured seat dimensions, see Table 4 for descriptions.

DOI: 10.13009/EUCASS2023-044

Table 4: Seat features size in [mm].

	Description	Seat A	Seat B	Goossens et al.[32]
a	Headrest height	19	19	NA
b	Distance between SRP and center of headrest	77	77	NA
c	Backrest height	60	60	65 min
d	Armrest height	NA	27	20-32
e	Seat depth	43	50-52	41-45
f	Seat height	45	45-55	33-51
g	Armrest length	NA	29	28 min
h	Armrest width	NA	7.5	6.5
i	Seat width effective	43	43	43 min
l	Headrest width	26	26	NA
m	Backrest width	43	45	43-46
n	Width between armrest	NA	52	47
α	Seat inclination from backrest	108	75-180	90
β	Backrest inclination	72	0-90	65-85
γ	Armrest inclination	NA	0-10	0-5

The measurements reported in Table 4 were compared with the references' comfortable values taken from the literature by Goossens et al.,[32] which mainly uses the Aerospace Standard AS290.[33] According to AS209, the backrest angle during flight should be between 65° and 85°. The MARTA FFS seat B is a flippable seatback, but the angle is maintained as the seat A with an angle of 75° (β in Figure 4). Not all of the measures considered in this work were used by Goossens et al.[32] and are therefore reported as Not Assigned (NA) in Table 4. It is worth stating that seat A does not have armrests.

The tests performed on both seats were carried out with two main payloads. The passengers in the experimental campaign were grouped. Three females with an equivalent mass of about 50 kg and three males of about 70 kg were selected and tested on both seats; more details on the passengers in terms of age, height, and weight are given in Table 5.

Table 5: Passengers' data characteristics, mean and (Standard Deviation).

Sex	**Age**	**Height**	**Weight**
Male	24.6 (2.3)	1.75 m (0.38)	68.8 kg (1.2)
Female	21.6 (0.8)	1.63 m (0.41)	49.6 kg (5.1)

The arrangement of the sensors is shown in Figure 3(b) and (c) for the two seats considered. Concerning data acquisition, four measuring points were used. Tri-axial accelerometers have been used in positions 1, 2, and 4. The accelerometers A1 and B1 were mounted in the structural frame of the seat. The accelerometers A2 and B2 were used to measure the accelerations on the feet area. The seat pad accelerometer is located on the seat surface, locations named A3 and B3, respectively. Since the positioning of the sensor in the middle of the backrest area it was not possible due to incompatibility with the contact surfaces, it was decided to place this sensor close to the cervical region (A4 and B4). For this reason, results referred to this area are reported under the label "seat-back". It is to be said that the weighting filters suggested by ISO 2631[34] for the backrest area are employed to elaborate the seat-back data.

Figure 5 shows an example of the arrangement of the accelerometers in the case of the business seat. The front view and back view are shown in Figure 5. Two different types of accelerometers were used in the set-up; the PCB Model 356B41 - Seat Pad Accelerometer is similar to a roughly cylindrical cushion with a size (Diameter x Thickness) of 200 mm x 12 mm and a weight of 272 g. This kind of accelerometer is used in the laboratory according to ISO 10326[35] standards. The sensors in the other measure locations are tri-axial accelerometers, PCB manufactured, model 356B18.

DOI: 10.13009/EUCASS2023-044

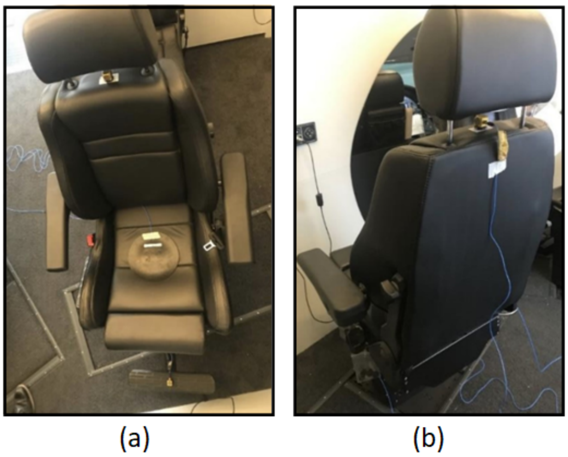

Figure 5: Example of accelerometers set-up. Seat B front view (a), Seat B back view (b).

3. Results

ISO 2631 presents several indexes based on the acquired acceleration data; in what follows, only the parameters considered for the analysis of results are illustrated. The WBV exposure parameters were calculated for each flight condition. The three principal areas of interest are the backrest, seat surface, and feet. As described, the seat configurations have been named A and B; the acronym SEAT A identifies the seat without armrest and footrest, while SEAT B represents the business seat configuration. Moreover, the code SEAT A 50, refers to seat A with a passenger weight of 50 kg. Last, all the acronyms used for the different flight phases are reported in Table 6.

Table 6: Acronyms of the flight segments.

Flight phase	**Named**
Take-off	TO
Cruise without Turbulence	C1
Cruise with Turbulence	C2
Landing	LA

3.1 Average Weighted Vibration

The WBV exposure parameters considered will be discussed individually. The first one is the weighted root mean square acceleration, as defined by equation 1. The weighted r.m.s. acceleration is expressed over (m/s^2) for translational vibration and (rad/s^2) for rotational vibration.

$$a_w = \left[\frac{1}{T} \int_0^T a_w^2(t) \; dt \right]^{\frac{1}{2}} \tag{1}$$

In equation 1 $a_w(t)$ is the weighted acceleration (translational or rotational) as a function of time, and T is the duration of the measurement in seconds.
Acceptable values of vibration magnitude for comfort depend on many factors that vary with each application. For this reason, no limits are defined in IS0 2631. The following values, listed in Table 7, give an approximate range to evaluate the severity of the WBV exposure parameter a_w with respect to discomfort.
Based on collected data, it is possible to identify different behavior of the indexes by comparing the flight phases and between the two seat configurations. Similar results were found for both payload configurations.
Considering the take-off phase for both seats, Table 8 lists the results for the passengers' payload equal to 50 kg and 70 kg, for the three different areas. Analyzing the acceleration along the three axes, it is easy to identify the prevalence of the component along the z-axis for all the measuring positions. Particular attention should be paid to the position sensor in the seat-back, as the component along the x-axis is comparable in this case with the component along z-axis. This is due to the acceleration dose that the passenger receives during the take-off phase, which is essentially directed toward the backrest.

DOI: 10.13009/EUCASS2023-044

Table 7: Scale of vibratory discomfort from ISO 2631.

r.m.s weighted acceleration $[m/s^2]$	**(Dis)comfort reactions**
Less than 0.315	not uncomfortable
0.315 ÷ 0.63	a little uncomfortable
0.5 ÷ 1	fairly uncomfortable
0.8 ÷ 1.6	uncomfortable
1.25 ÷ 2.5	very uncomfortable
Greater than 2 m/s^2	extremely uncomfortable

Table 8: RMS for take-off flight segment.

Take-off "TO"	a_w **Feet** $[m/s^2]$			a_w **Seat-surface** $[m/s^2]$			a_w **Seat-back** $[m/s^2]$		
Axes	x	y	z	x	y	z	x	y	z
SEAT A 70	0.037	0.016	0.108	0.021	0.008	0.100	0.058	0.009	0.068
SEAT B 70	0.025	0.017	0.109	0.020	0.006	0.104	0.060	0.013	0.069
SEAT A 50	0.043	0.023	0.159	0.018	0.007	0.097	0.059	0.009	0.071
SEAT B 50	0.025	0.017	0.113	0.018	0.006	0.121	0.066	0.013	0.072

Similar comments regarding Tables 9 and 10 for the cruise phase with turbulence and the landing phase concerning the vibration dose along the z-axis can be made. In Table 9, additionally, with reference to the component along the z-axis of the backrest (Seat-back), it is possible to notice the higher RMS values on overall acquisition points and flight phases, essentially due to the turbulence effects.

Table 9: RMS for a cruise with turbulence flight segment.

Cruise "C2"	a_w **Feet** $[m/s^2]$			a_w **Seat-surface** $[m/s^2]$			a_w **Seat-back** $[m/s^2]$		
Axes	x	y	z	x	y	z	x	y	z
SEAT A 70	0.056	0.047	0.114	0.055	0.052	0.128	0.067	0.048	0.231
SEAT B 70	0.058	0.061	0.105	0.073	0.074	0.118	0.062	0.057	0.221
SEAT A 50	0.060	0.050	0.120	0.055	0.054	0.131	0.069	0.050	0.242
SEAT B 50	0.055	0.058	0.104	0.070	0.069	0.118	0.065	0.054	0.211

Table 10: RMS for landing flight segment.

Landing "LA"	a_w **Feet** $[m/s^2]$			a_w **Seat-surface** $[m/s^2]$			a_w **Seat-back** $[m/s^2]$		
Axes	x	y	z	x	y	z	x	y	z
SEAT A 70	0.051	0.049	0.293	0.033	0.028	0.197	0.088	0.026	0.103
SEAT B 70	0.058	0.063	0.327	0.036	0.037	0.259	0.210	0.050	0.119
SEAT A 50	0.057	0.057	0.312	0.036	0.032	0.212	0.096	0.031	0.105
SEAT B 50	0.063	0.062	0.343	0.038	0.032	0.301	0.194	0.053	0.122

Focusing on the component along the z-axis during the take-off (Table 8) and the landing phase (Table 10), it is possible to highlight a further similarity. In both flight phases the a_w value calculated in the position of the feet is greater than that calculated in the seat surface. The result is similar for both seat configurations.
What is found during the take-off and landing phase is that the indexes computed for the business seat (SEAT B) are greater than the ones of the flight attendance class (SEAT A). In those cases, it would seem that the feet support frame structure available to the business passenger amplifies the transmitted vibrations. On the other hand, during the cruising phase with turbulence (Table 9) it can be seen that the SEAT B has lower values than the SEAT A. This converts into a greater sensation of comfort for the passenger.
Concerning the indexes computed for the z-axis component at the seat surface, the results lead to similar conclusions for both passenger groups. These are shown in Figure 6 (a) and (b), respectively. Exception made for the cruise phase, the indexes are higher for the business seat configuration with respect to the attendance configuration. The result is essentially ascribed to the fixture frame, which is different for the two configurations, as it appears from Figure 3. In each case, as stated in the scale of vibratory discomfort from ISO 2631 (refer to Table 7), the WBV that the passenger

DOI: 10.13009/EUCASS2023-044

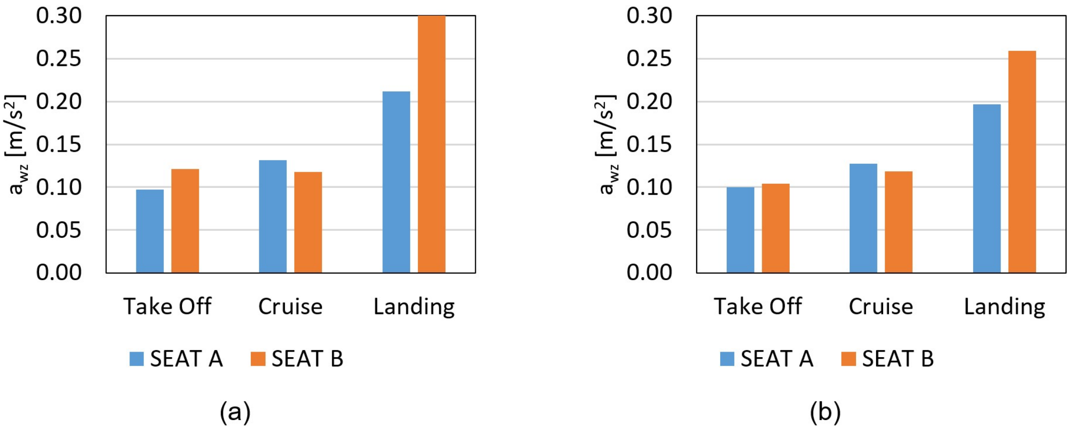

Figure 6: Seat-surface a_{wz} classified for seat configuration in terms of passenger payload 50 kg (a) and 70 kg (b).

would feel during the different phases is comfortable because less than 0.315 m/s^2. It is worth knowing that taking into account the aforementioned index values, the flight experience can be classified as "not uncomfortable".

3.2 Vibration Total Value

The vibration total value of weighted RMS is obtained by combining vibrations in more than one direction, determined from vibration in orthogonal coordinates as equation 2:

$$a_v = \left(k_x^2\, a_{wx}^2 + k_y^2\, a_{wy}^2 + k_z^2\, a_{wz}^2\right)^{\frac{1}{2}} \tag{2}$$

where multiplying factors k values are listed in Table 11 along with the weighting frequency filters W according to ISO 2631 to be considered in each orthogonal direction, in case of seated persons, for the three areas of interest: supporting seat surface, backrest and feet, respectively.

Table 11: Frequency weightings and multiplying factors defined in ISO 2631.

	Seat surface	**Backrest**	**Feet**
k_x	1	0.8	0.25
k_y	1	0.5	0.25
k_z	1	0.4	0.4
x-axis	W_d	W_c	W_k
y-axis	W_d	W_d	W_k
z-axis	W_k	W_d	W_k

Based on the fact that the most severe WBV parameters were found during the landing phase, from the analysis of average weighted acceleration indexes, in Figure 7, results of vibration total value focused on this flight phase are shown. In particular, Figure 7 refers to the three different measuring areas. Considering that a_v parameter involves the orthogonal coordinates, the results have higher values for the seat surface. In the same figure, we distinguish the behavior of the two different seats and the results for the two classes of tested passengers. An increase in passenger mass, from 50 kg to 70 kg, in both seats reduces the obtained parameters. However, also in this case, as we recognized from the results obtained previously for the average weighted vibration, the business configuration is less comfortable during the investigated flight phases, at least from a mere quantitative acceleration measure during the landing maneuvers.

DOI: 10.13009/EUCASS2023-044

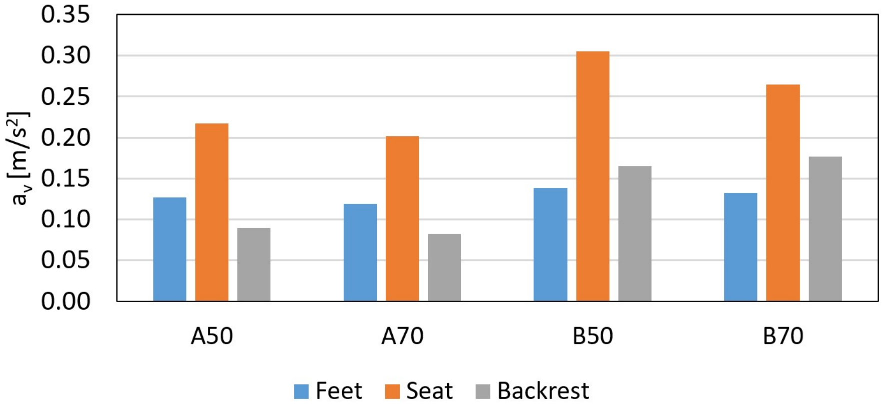

Figure 7: Vibration Total Value "a_v" for the landing phase.

3.3 Vibration Dose Value

The modulus of the ratio of the maximum instantaneous peak value of the frequency-weighted acceleration signal to its rms value is defined as the "crest factor" by ISO 2631. When this ratio is higher than 9 it is recommended to use the Vibration Dose Value (VDV) instead of the weighted rms value. The fourth power VDV in meters per second to the power 1.75 ($m/s^{1.75}$) is defined by the equation 3:

$$VDV = \left\{ \int_0^T [a_w(t)]^4 \; dt \right\}^{\frac{1}{4}} \tag{3}$$

where $a_w(t)$ is the instantaneous frequency-weighted acceleration and T is the duration of the measurement. By using the fourth power instead of the second power of the acceleration time history as the basis for averaging, the index is more sensitive to peaks than the basic evaluation method. Regarding the data acquired, the crest factor is greater than 9 for the take-off and landing phases, while for the cruising phase equals 4. Thus, such signals should also be analyzed in terms of the VDV for the considered flight phases.

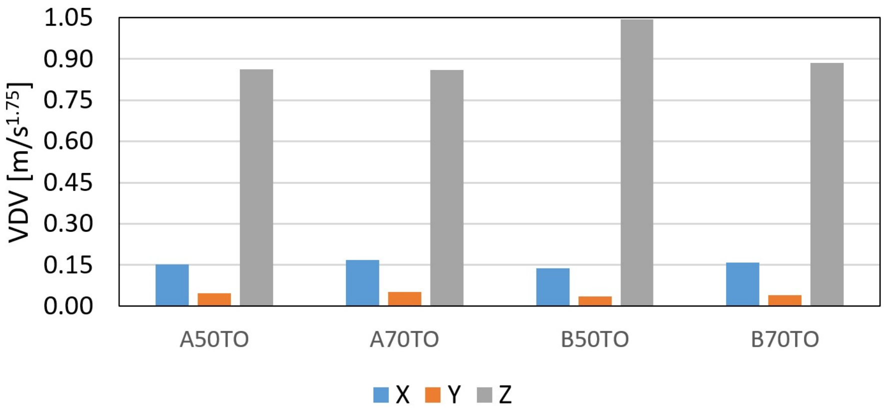

Figure 8: Vibration Dose Value during take-off.

As computed for the weighted root mean square acceleration, data obtained for VDV are shown in Figure 8 for the take-off phase. It is possible to acknowledge that the z-axis component is clearly prevalent with respect to the others. Similar results were obtained for the other analyzed flight phases.
In Figure 9, the influence of the seat configuration and of the flight phases in terms of z axis component for the seat pad surface sensor are reported. As previously discussed, the accelerations along z are the main component, for this reason only the VDV_z is shown. It is confirmed that the amount of acceleration dose during the landing phase is predominant compared to the take-off and cruise, mainly due to the acceleration induced by the touchdown.

DOI: 10.13009/EUCASS2023-044

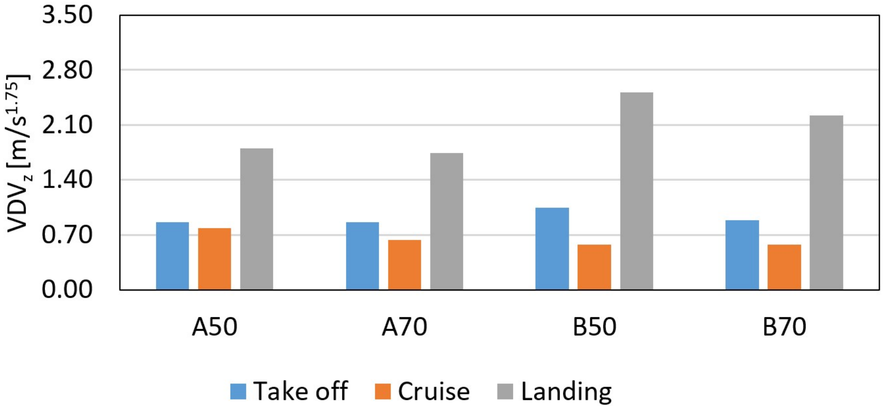

Figure 9: Vibration Dose Value for the fight phases.

4. Conclusions

The proposed experimental campaign has allowed the measurement of the objective comfort indexes provided by the ISO 2631 standard. The use of FFS offers unique opportunities to create ad hoc mock-ups to satisfy the design philosophy of a human-centered cabin interior without using a real aircraft for such purposes, interfacing objective data with the subjective feeling of the passenger in a simulated environment similar to the real aircraft, which can also reproduce personal audio and visual stimuli, unlike the multi-axis shaking tables. Analysis of the results has highlighted the following.
Although the acceleration levels are comparable with data from the literature, and a cruise phase with moderate turbulence with a higher energy amount is tested, the comfort indexes are lower than the limits suggested by the regulations. The results have detected the behavior of two different seats. Globally, the business configuration seat B indexes are worse than seat A. This result depends on the fact that the parameters analyzed are entirely objective and contingent on the stiffness characteristics of the whole system. The indexes also do not consider the subjective aspects of the seats, such as armrests, seat dimensions, and ergonomics. These subjective evaluations will be the object of future research activities.
From a bibliographic analysis of the literature, it was found that there are no relevant tests experienced on full motion type D flight simulators; therefore based on the acquired signals, the estimation of new additional comfort indexes taking into account the particular cue is suitable.

Informed consent

Informed consent was obtained from all subjects involved in the study. The study was conducted in accordance with the Declaration of Helsinki, and approved by the Ethics Committee of Kore University Enna (protocol code 2510 and date of 04/02/2022).

Acknowledgments

The study was financially supported by the Italian Ministry of University and Research - M.U.R. under the AGREED project (P.O.N. Grant ARS01_00254).

References

[1] Council of European Union. Council regulation (EU) no 44/2002, 2002.

[2] Bengt-Olov Wikström, Anders Kjellberg, and Ulf Landström. Health effects of long-term occupational exposure to whole-body vibration: a review. *International Journal of Industrial Ergonomics*, 14(4):273–292, 1994.

[3] S Lings and C Leboeuf-Yde. Whole-body vibration and low back pain: a systematic, critical review of the epidemiological literature 1992–1999. *International archives of occupational and environmental health*, 73(5):290–297, 2000.

DOI: 10.13009/EUCASS2023-044

[4] Cho-Chung Liang and Chi-Feng Chiang. A study on biodynamic models of seated human subjects exposed to vertical vibration. *International Journal of Industrial Ergonomics*, 36(10):869–890, 2006.

[5] Prasad Bhagwan Kumbhar, Peijun Xu, and Jingzhou Yang. A literature survey of biodynamic models for whole body vibration and vehicle ride comfort. In *International Design Engineering Technical Conferences and Computers and Information in Engineering Conference*, volume 45059, pages 671–687. American Society of Mechanical Engineers, 2012.

[6] James L Coyte, David Stirling, Haiping Du, and Montserrat Ros. Seated whole-body vibration analysis, technologies, and modeling: a survey. *IEEE Transactions on Systems, Man, and Cybernetics: Systems*, 46(6):725–739, 2015.

[7] Subhash Rakheja, Krishna N Dewangan, Ren G Dong, Pierre Marcotte, and Anand Pranesh. Whole-body vibration biodynamics-a critical review: Ii. biodynamic modelling. *International Journal of Vehicle Performance*, 6(1):52–84, 2020.

[8] Mike Kolich, Steven D. Essenmacher, and James T. McEvoy. Automotive seating: the effect of foam physical properties on occupied vertical vibration transmissibility. *Journal of Sound and Vibration*, 281(1):409–416, 2005.

[9] H Ciloglu, M Alziadeh, A Mohany, and H Kishawy. Assessment of the whole body vibration exposure and the dynamic seat comfort in passenger aircraft. *International Journal of Industrial Ergonomics*, 45:116–123, 2015.

[10] Linchuan Guo, Xu Wang, Rang-Lin Fan, and Fengrong Bi. Review on development of high-static-low-dynamic-stiffness seat cushion mattress for vibration control of seating suspension system. *Applied Sciences*, 10(8), 2020.

[11] Makoto Futatsuka, Setsuo Maeda, Tsukasa Inaoka, Megumi Nagano, Masahiro Shono, and Takashi Miyakita. Whole-body vibration and health effects in the agricultural machinery drivers. *Industrial health*, 36(2):127–132, 1998.

[12] Jan Ivar Kåsin, Neil Mansfield, and Anthony Wagstaff. Whole body vibration in helicopters: risk assessment in relation to low back pain. *Aviation, space, and environmental medicine*, 82(8):790–796, 2011.

[13] Aykut Tamer, Vincenzo Muscarello, Giuseppe Quaranta, and Pierangelo Masarati. Cabin layout optimization for vibration hazard reduction in helicopter emergency medical service. *Aerospace*, 7(5):59, 2020.

[14] Ornwipa Thamsuwan, Ryan P Blood, Randal P Ching, Linda Boyle, and Peter W Johnson. Whole body vibration exposures in bus drivers: A comparison between a high-floor coach and a low-floor city bus. *International Journal of Industrial Ergonomics*, 43(1):9–17, 2013.

[15] A Bekker, KI Soal, and KJ McMahon. Whole-body vibration exposure on board a polar supply and research vessel in open water and in ice. *Cold Regions Science and Technology*, 141:188–200, 2017.

[16] Bazil Basri and Michael J Griffin. The application of seat values for predicting how compliant seats with backrests influence vibration discomfort. *Applied ergonomics*, 45(6):1461–1474, 2014.

[17] Thomas K Dempsey, Jack D Leatherwood, and Sherman A Clevenson. Development of noise and vibration ride comfort criteria. *The Journal of the Acoustical Society of America*, 65(1):124–132, 1979.

[18] Andrea Zanoni, Alessandro Cocco, and Pierangelo Masarati. Multibody dynamics analysis of the human upper body for rotorcraft-pilot interaction. *Nonlinear Dynamics*, 102(3):1517–1539, 2020.

[19] Suzanne D Smith. Dynamic characteristics and human perception of vibration aboard a military propeller aircraft. *International Journal of Industrial Ergonomics*, 38(9-10):868–879, 2008.

[20] Peter Vink, C Bazley, Irene Kamp, and Merle Blok. Possibilities to improve the aircraft interior comfort experience. *Applied ergonomics*, 43(2):354–359, 2012.

[21] Antonio Esposito, Calogero Orlando, and Andrea Alaimo. Cabin aircraft comfort evaluation over high fidelity simulated flight. *CEAS Aeronautical Journal*, pages 1–18, 2023.

[22] Neil J Mansfield. *Human response to vibration*. CRC press, 2004.

[23] Patrik Holmlund and Ronnie Lundström. Mechanical impedance of the sitting human body in single-axis compared to multi-axis whole-body vibration exposure. *Clinical Biomechanics*, 16:101–110, 2001.

DOI: 10.13009/EUCASS2023-044

[24] Neil J Mansfield and Setsuo Maeda. The apparent mass of the seated human exposed to single-axis and multi-axis whole-body vibration. *Journal of Biomechanics*, 40(11):2543–2551, 2007.

[25] A Esposito, F Lo Iacono, C Orlando, G Navarra, and A Alaimo. Whole body vibration during simulated flight via uncertain models and interval analysis. *Mechanics of Advanced Materials and Structures*, pages 1–10, 2022.

[26] Francesco Lo Iacono, Andrea Alaimo, Antonio Esposito, Giacomo Navarra, and Calogero Orlando. An anthropometric 4-dof vibration model with uncertain parameters for air transportation. In *AIP Conference Proceedings*, volume 2293, page 200008. AIP Publishing LLC, 2020.

[27] Behrang Keshavarz. Exploring behavioral methods to reduce visually induced motion sickness in virtual environments. In Stephanie Lackey and Randall Shumaker, editors, *Virtual, Augmented and Mixed Reality*, pages 147–155, Cham, 2016. Springer International Publishing.

[28] John J Catherines, John S Mixson, and Harland F Scholl. Vibrations measured in the passenger cabins of two jet transport aircraft. Technical report, 1975.

[29] John C. Houbolt. Atmospheric turbulence. *AIAA Journal*, 11(4):421–437, 1973.

[30] Andrea Alaimo, Antonio Esposito, and Calogero Orlando. Cockpit pilot warning system: a preliminary study. In *2018 IEEE 4th International Forum on Research and Technology for Society and Industry (RTSI)*, pages 1–4. IEEE, 2018.

[31] Andrea Alaimo, Antonio Esposito, Palmira Faraci, Calogero Orlando, and Giusy Danila Valenti. Human heart-related indexes behavior study for aircraft pilots allowable workload level assessment. *IEEE Access*, 10:16088–16100, 2022.

[32] R.H.M Goossens, C.J Snijders, and T Fransen. Biomechanical analysis of the dimensions of pilot seats in civil aircraft. *Applied Ergonomics*, 31(1):9–14, 2000.

[33] Aerospace standard as290a seats for flight deck crewmen - transport aircraft. Standard, Society of Automotive Engineers, Warrendale, PA, USA, 1971.

[34] Iso 2631-1:1997 - mechanical vibration and shock - evaluation of human exposure to whole-body vibration - part 1: General requirements. Standard, International Organization for Standardization, Geneva, CH, 1997.

[35] Iso10326-1:2016 - mechanical vibration - laboratory method for evaluating vehicle seat vibration - part 1: Basic requirements. Standard, International Organization for Standardization, Geneva, CH, 2016.